

EXPRESS LETTER

Open Access



Climatology of mesosphere and lower thermosphere diurnal tides over Jicamarca (12°S, 77°W): observations and simulations

Jose Suclupe^{1*} , Jorge L. Chau¹, J. Federico Conte¹, Marco Milla², N. M. Pedatella³ and K. Kuyeng⁴

Abstract

This work shows a 3-year climatology of the horizontal components of the solar diurnal tide, obtained from wind measurements made by a multistatic specular meteor radar (SIMONE) located in Jicamarca, Peru (12°S, 77°W). Our observations show that the meridional component is more intense than the zonal component, and that it exhibits its maxima shifted with respect to the equinox times (i.e., the largest peak occurs in August–September, and the second one in April–May). The zonal component only shows a clear maximum in August–September. This observational climatology is compared to a climatology obtained with the Whole Atmosphere Community Climate Model with thermosphere and ionosphere extension (WACCM-X). Average comparisons indicate that the model amplitudes are 50% smaller than the observed ones. The WACCM-X results are also used in combination with observed altitude profiles of the tidal phases to understand the relative contributions of migrating and non-migrating components. Based on this, we infer that the migrating diurnal tide (DW1) dominates in general, but that from June until September (November until July) the DE3 (DW2) may have a significant contribution to the zonal (meridional) component. Finally, applying wavelet analysis to the complex amplitude of the total diurnal tide, modulating periods between 5 and 80 days are observed in the SIMONE measurements and the WACCM-X model. These modulations might be associated to planetary waves and intraseasonal oscillations in the lower tropical atmosphere.

Keywords Climatology, Diurnal tide, Low latitude, Tidal modulation, Meteor radar, GCM

*Correspondence:

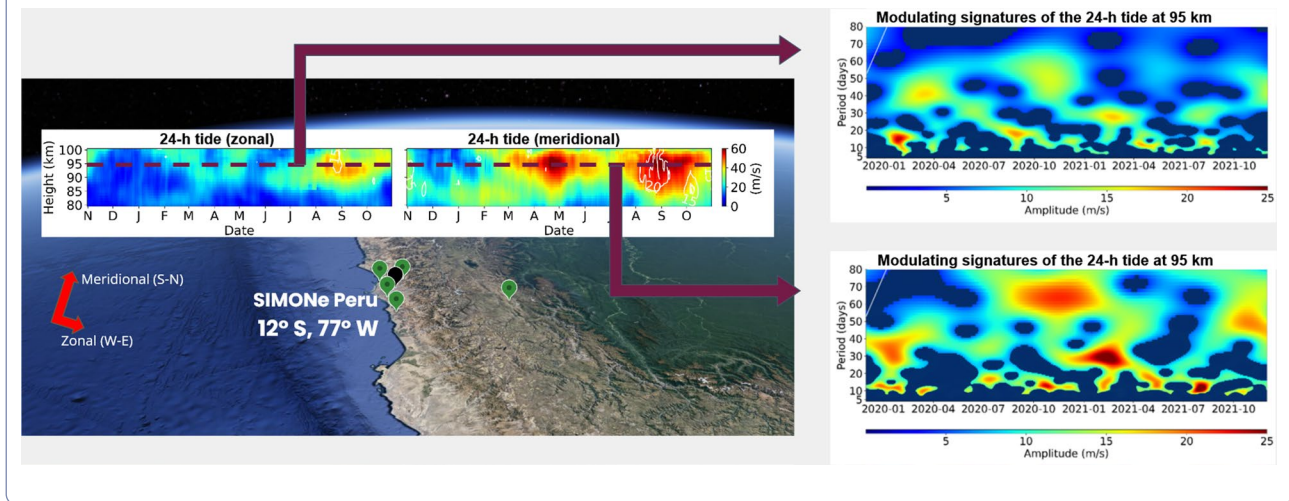
Jose Suclupe
suclupe@iap-kborn.de

Full list of author information is available at the end of the article



© The Author(s) 2023. **Open Access** This article is licensed under a Creative Commons Attribution 4.0 International License, which permits use, sharing, adaptation, distribution and reproduction in any medium or format, as long as you give appropriate credit to the original author(s) and the source, provide a link to the Creative Commons licence, and indicate if changes were made. The images or other third party material in this article are included in the article's Creative Commons licence, unless indicated otherwise in a credit line to the material. If material is not included in the article's Creative Commons licence and your intended use is not permitted by statutory regulation or exceeds the permitted use, you will need to obtain permission directly from the copyright holder. To view a copy of this licence, visit <http://creativecommons.org/licenses/by/4.0/>.

Graphical Abstract



Introduction

The mesosphere and lower thermosphere (MLT) is the transition region between the lower atmosphere and the ionosphere/thermosphere. As such, the MLT is pierced by a myriad of waves with different periods and scales. Among them, solar tides are prominent and are essential contributors to the large-scale dynamics and energy budget of the MLT (e.g., Smith 2012).

Solar tides have periods of 24, 12, 8 h and other sub-harmonics of a solar day. They are mainly excited by the latent heat release and the absorption of near-infrared radiation by the water vapor in the troposphere and the absorption of UV radiation by the ozone in the stratosphere (e.g., Forbes 1995; Hagan and Forbes 2003). Tides can be further classified into migrating and non-migrating. Migrating tides are sun-synchronous, that is, they propagate westward following the apparent movement of the Sun. Non-migrating tides are not sun-synchronous; they can be eastward- or westward-propagating or stationary. These non-migrating tidal components have different sources, such as longitudinal variation in the diurnal heating and non-linear interactions between planetary waves and migrating tides (e.g., Hagan 1996). A typical notation is [period][direction of phase propagation][wavenumber]; for instance, DW1 refers to the diurnal (24-h) tide, westward-propagating with wavenumber $k = 1$. As the tides propagate vertically towards the upper atmosphere, they may be modulated by, e.g., planetary waves (e.g., Laštovička 2006). On the other hand, lunar tides (waves with periods of 12.42 h) have also been reported at low latitudes with relatively weak but significant amplitudes (e.g., Sandford and Mitchell 2007).

Planetary waves have periods from a couple of days to ~30 days, and horizontal scales of several thousand km. A well-known observed planetary wave that achieves large amplitudes in the MLT region is the quasi-two-day wave (Q2DW) (e.g., Smith 2012; He et al. 2021).

Characterizing the climatology of the dominant large-scale waves at MLT altitudes is important to improve the understanding of atmospheric mean global dynamics. In this work, we contribute to that goal with (a) a climatology of horizontal background winds, the Q2DW, and solar tides (24, 12, and 8 h) over the central coast of Peru (Jicamarca—12°S, 77°W), and the comparison of this observational climatology with that obtained from the WACCM-X model; (b) a discussion of the possible wavenumbers contributing to the total 24-h tide observed at Jicamarca; and (c) a report of the main periods modulating the diurnal tide observed over Jicamarca.

This paper is structured as follows. The used data sets are described in "Dataset" Section. The methodology implemented to post-process the data sets is presented in "Methods" Section. In "Results" Section, the observed and simulated results are presented, which are later discussed in "Discussion" Section. Finally, the concluding remarks are given in "Concluding Remarks" Section.

Data set

The observational data set used in this work comprises zonal and meridional winds with resolutions of 1-h, and 2-km between October 2019 and January 2023. These winds were estimated every 30 min and 1 km (sampling) between 80 and 100 km of altitude, using

the homogeneous method (e.g., Conte et al. 2021). They were estimated from measurements made by the multistatic meteor radar SIMONE (Spread-spectrum Interferometric Multistatic meteor radar Observing Network) deployed around the Jicamarca Radio Observatory (11.95°S, 76.87°W SIMONE Jicamarca) (Chau et al. 2021). This system has a horizontal coverage of approximately 400 km in diameter.

The simulated winds consist of two data sets of zonal and meridional winds from the WACCM-X (Whole Atmosphere Community Climate Model with thermosphere–ionosphere eXtension) model. WACCM-X results are based on the Specified Dynamics configuration where the model meteorology is constrained by MERRA-2 up to ~ 50 km. Detailed information about this model data set and WACCM-X can be found in Pedatella et al. (2021) and references therein. The first data set covers the period January 2010–February 2020 and is provided for a latitude of 11.95°S, every 3 h, 5 degrees in longitude (from 0° to 355°), and ~2 km altitude resolution at MLT altitudes. This data set was used to get the climatology. The second data set spans the period November 2019–December 2021, and is provided at 12.3°S, 77.5°W, every 3 h, and was used to investigate the modulation of the 24-h tide in the model.

Methods

One well-known method to extract wave information (amplitude and phase) in wind data is least squares. We use this method to get the mean background wind, amplitudes of tides and Q2DW, and obtain the diurnal tide’s phase profiles.

The least squares method allows for the selection and fitting of specific harmonic components. Furthermore, this method has the advantage of not being affected by data gaps, i.e., the time series is not required to be equally spaced.

For M dominant harmonic components, the time series $x(t_n)$, $n = 1, 2, 3, \dots, N$, can be expanded as

$$\begin{aligned} x(t_n) &= \bar{x} + \sum_{q=1}^M C_q \cos(2\pi f_q t_n - \phi_q) + x_r(t_n) \\ &= \bar{x} + \sum_{q=1}^M [A_q \cos(2\pi f_q t_n) \\ &\quad + B_q \sin(2\pi f_q t_n)] + x_r(t_n), \end{aligned} \tag{1}$$

where \bar{x} is the mean value; t_n is the time; C_q , f_q , and ϕ_q are the amplitude, frequency, and phase of the q th harmonic, respectively ($q = 1, 2, \dots, M$); and x_r is the residual, which

may contain the contributions from unfitted harmonics. Once the coefficients are estimated, the amplitude C_q and the phase ϕ_q of each specified component are calculated as

$$C_q = (A_q^2 + B_q^2)^{1/2}; \phi_q = \tan^{-1}(B_q/A_q) \tag{2}$$

The size of the fitting window must be such that it allows for resolving the frequencies of interest. The frequency resolution is given by: $\Delta f = \frac{f_s}{N} = \frac{1}{N\Delta t}$, where f_s is the sampling frequency, Δt is the sampling time and N is the number of samples. Since Δt is fixed, then an appropriate value of N must be chosen (i.e., a proper window size $N\Delta t$) to have an adequate separation of the frequencies to be studied (e.g., Conte et al. 2017).

In this work, the fitted amplitudes $C_q > 0$ (given in equation 2) are used to analyze the climatology, and the phase profiles ϕ_q are used to infer the migrating and non-migrating diurnal tide contributions. On the other hand, the next complex time series is defined using the fitted A_q and B_q given in (2):

$$C_{q,complex} = A_q - jB_q, \tag{3}$$

Then, $C_{q,complex}$ is taken as the input of the Continuous Wavelet Transform (CWT) to investigate the modulation of the 24-h tide. This modulation of the tide is considered a non-linear wave–wave interaction, similar to an amplitude modulation problem where the carrier signal is the diurnal tide and the modulating signals are large-period oscillations whose frequencies we desire to recover.

This complex “amplitude” ($C_{q,complex}$) was here defined because it is equivalent to the “complex envelope” defined in the context of the Hilbert Transform (Chapter 4., Feldman 2011). The spectrum of the complex envelope has the same frequency and amplitude information as the modulating signal’s spectrum but with a shifted phase, allowing recovery the modulating periods. See Annex 1 for details on the latter and Annex 2 for details on the CWT implementation.

Results

Climatology of SIMONE observations

The least squares method described in the previous section was implemented with bins of 21 days shifted by 1 day at each given altitude. This was done to both the observed and simulated data, with the purpose of estimating the mean wind and the total amplitudes of the tides with periods 8, 12, 12.42, and 24 h as well as the Q2DW with a period of 48 h. The size of the fitting window was selected equal to 21 days to separate the contributions from the 12-h solar tide and the lunar tide of period 12.42 h. In this way, any contamination of the 12-h

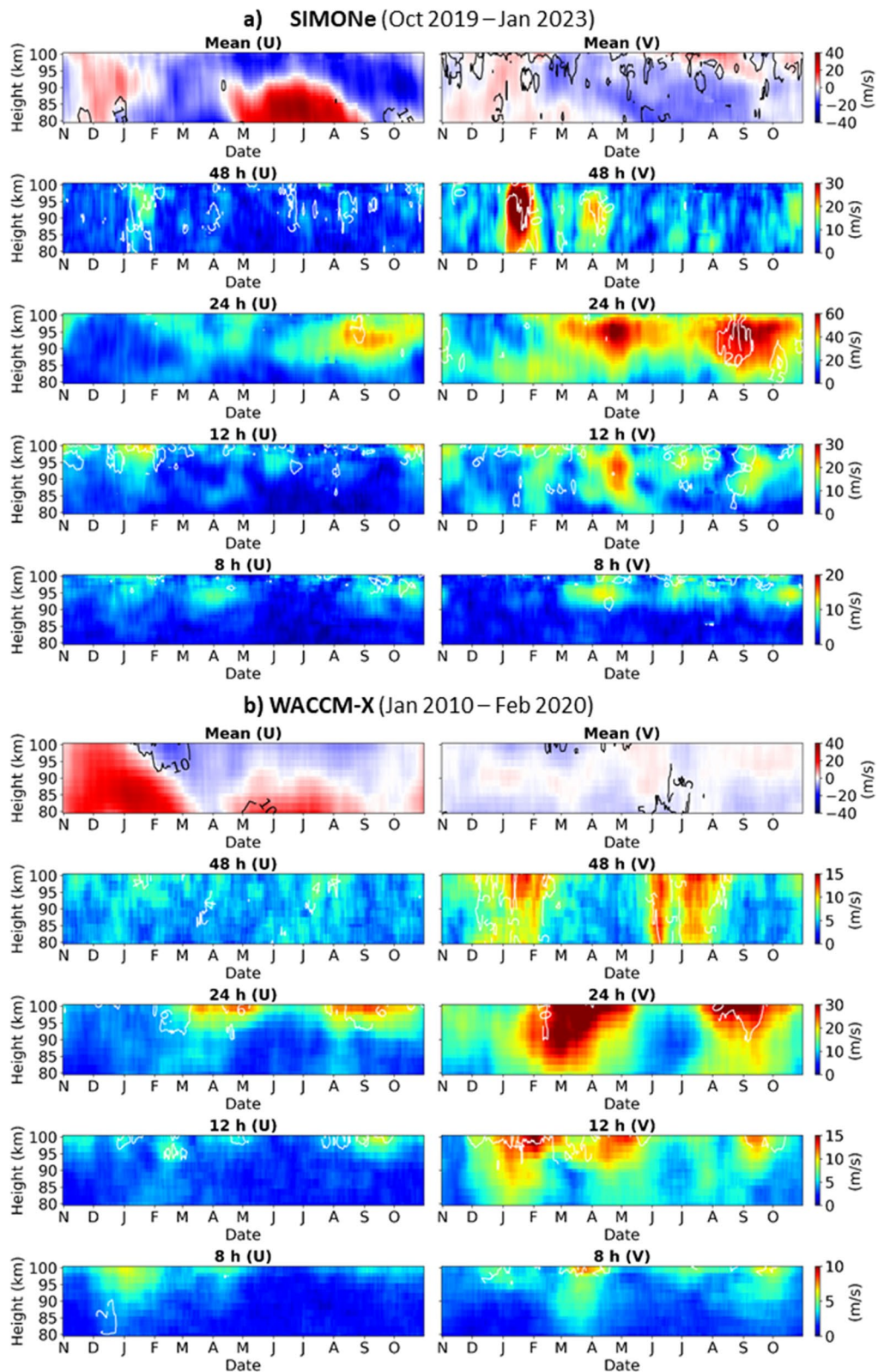


Fig. 1 Composite year of **a)** SIMONE observations, and **b)** WACCM-X model for the zonal (left column) and meridional (right column) of the mean winds (first row) and amplitudes of the Q2DW (second row), the 24-h, 12-h and 8-h total tides (fourth, fifth and sixth rows, respectively). The contour lines indicate the areas with maximum inter-annual variability

solar tide by the 12.42-h lunar tide is reduced significantly (Chau et al. 2015).

To obtain the annual climatology of the estimated quantities at Jicamarca, their daily values were averaged over a period of 3 years and 4 months for SIMONE, and over 10 years and 2 months, in the case of the WACCM-X. The result of this average, called a composite year, is shown in Figs. 1a and 1b for the observations (SIMONE) and the model simulations (WACCM-X), respectively. The left column is used for the zonal component and the right for the meridional one. It should be noted that the SIMONE's color bar is twice the WACCM-X's color bar for the tides and the Q2DW. In addition, the unbiased standard deviation of the values used in the calculation of the composite year was computed, and their maxima are shown as white contour lines. This was done to highlight the time intervals and altitudes with maximum inter-annual amplitude variability. The climatology of the lunar tide exhibits amplitudes of less than 10 m/s, which are small compared to those of the other tidal components. For this reason, we do not include them in this work.

From Fig. 1a, it can be seen that

- Except in the case of the mean winds, the meridional component is more intense than the zonal one.
- In general, the 24-h tide is the most intense of all fitted waves.
- Regarding the mean zonal wind, a quasi-semiannual period is observed below 93 km and a quasi-annual one above. The largest eastward values (35 m/s) are observed during June, between 80 and 87 km. From April to early August, the mean zonal wind is mainly eastward between 80 and 93 km, and westward above 94 km. Between 80 and 100 km, the mean zonal wind is mostly eastward-directed in November–December and westward-directed in February–March and September–October. The most significant inter-annual amplitude variability (15 m/s) for the zonal mean wind is observed between 80 and 85 km from September 15 to October 15, from November 15 to 30, and from December 20 to 31.
- Regarding the mean meridional wind, it is mainly northward-directed from November to January for altitudes between 80 and 100 km. For the rest of the months, this wind component is southward-directed, except above 92 km from July to October, where it blows northward.
- The Q2DW reaches maximum intensity during the local summer months (mainly in January). The meridional component reaches a second intensity peak from March 15 until April 15 between 86 and 96 km. These two peaks show higher inter-annual amplitude variability (10 m/s) above 90 km.

- Regarding the meridional component of the 24-h tide, there are signatures from February to October with peaks mainly between 90 and 100 km. The maximum amplitudes are observed during August–September. There is a second peak in April–May. Note that during August and the first days of October, there is a high standard deviation value (15 and 20 m/s) which indicates inter-annual variability. Our observations show a shifted seasonal behavior with respect to equinox times in the meridional component with maxima in August–September and April–May.
- For the meridional 12-h tide, there are signatures between February and November, mainly above 85 km. The main peak occurs from April 15 to May 10 between 85 and 100 km. This peak coincides with that of the 24-h tide (mentioned above). For the zonal 12-h tide, signatures are observed from October until January and in June, mainly above 90 km, with one maximum in October between 95 and 100 km and another one in January between 90 and 100 km. At these maxima, the zonal component is twice the meridional one. Inter-annual amplitude variability is found above 93 km for both the zonal (5 m/s) and meridional (6 m/s) components.
- For the zonal and meridional 8-h tidal components, non-negligible amplitudes are observed above 90 km. The maximum values in both components are seen between March and April and in September–October.

Comparison with WACCM-X

The comparison of the SIMONE climatology (Fig. 1a) with that obtained using the WACCM-X data set (Fig. 1b) shows that

Table 1 Correlations and amplitude ratios of the climatology of mean winds and tides obtained from SIMONE observations and the WACCM-X model

	Zonal		Meridional	
	Correlation	Ratio	Correlation	Ratio
Mean wind	0.4	1.3	0.1	2.9
Q2DW	0.1	1.3	0.3	1.7
24-h tide	0.4	2.1	0.4	1.9
12-h tide	0.0	2.1	0.2	1.6
8-h tide	0.5	1.9	0.4	1.7
Average	0.3	1.7	0.3	2.0

The highest correlations are shown in bold

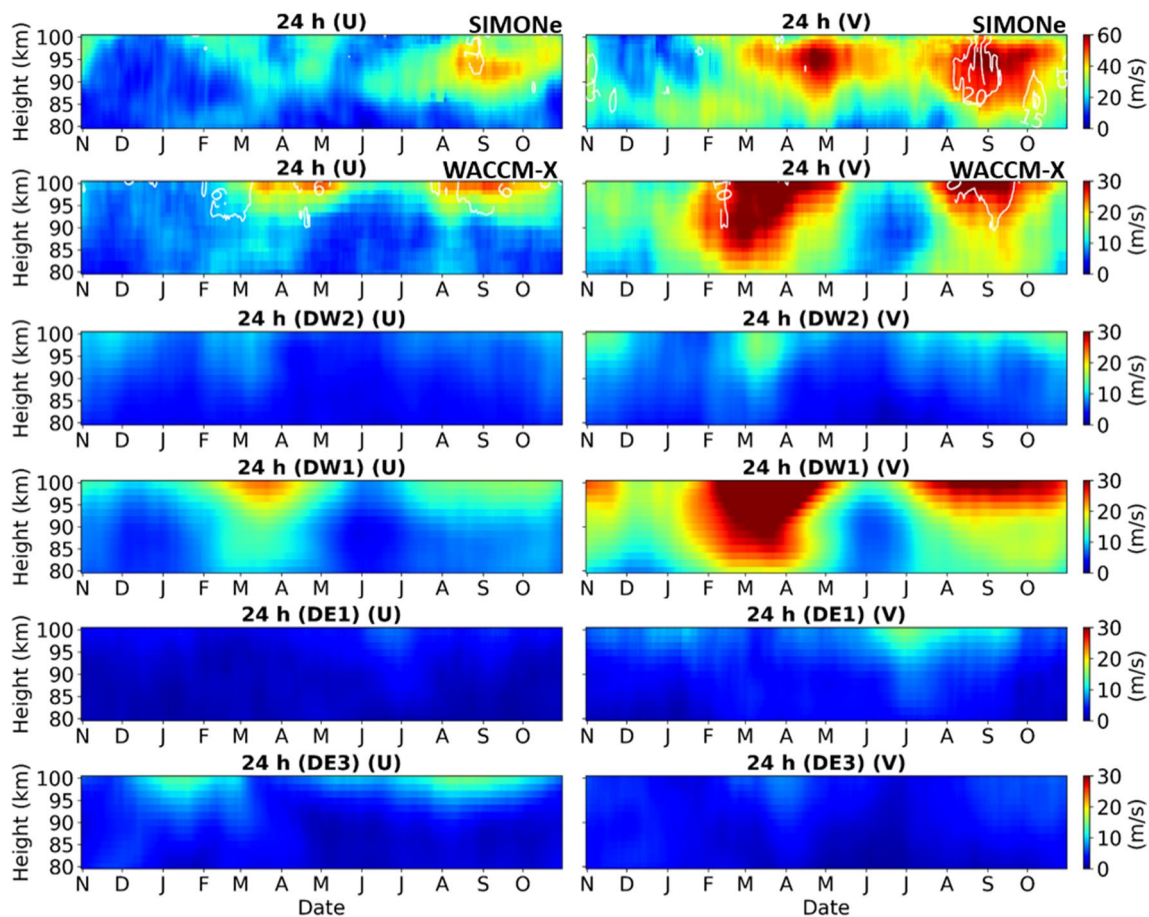


Fig. 2 Composite year of amplitudes of the zonal (left column) and meridional (right column) 24-h tides. From top to bottom, total tide obtained from SIMONE, and total tide, DW2, DW1, DE1, and DE3 extracted from WACCM-X

- The observations present amplitudes twice as large as the model.
- The model and the observations have no similarity in their mean meridional wind and are partially alike in the case of the mean zonal wind.
- For the model tides, amplitudes increase with height; this is not necessarily the case in the observations, where some waves maximize around 95 km.
- The observations show that the Q2DW has its maximum in January, while the model shows maxima during the local summer months (January), but also during the local winter months (beginning of June and July).
- For the meridional component of the 24-h tide, the observations show two similar peaks between August–September and April–May. Moreover, the model shows two peaks, the first between August and September and the second between February and April. For the zonal component of the 24-h tide, the observations show a peak between August and September. The model shows two similar peaks between August–September and March–April above 90 km.
- For the meridional component of the 12-h tide, observations show that it has its maximum amplitude in April–May. In contrast, the model shows three amplitude peaks, the first in January–February, the second in April–May, and the third in September.
- For the meridional component of the 8-h tide, similarly to the observations, the model shows amplitude increases in March–April and between September and October. For the zonal component, the observations show signatures in September–October and March–April, and a signature with less amplitude in December–January, while the model shows a maximum in December–January and less clear signatures in March–April and September–October.
- Correlations between the observed and simulated results presented in Fig. 1 have been estimated for each altitude and then averaged over all altitudes. Table 1 shows these correlations and the amplitude ratios. The amplitude ratio is calculated as the divi-

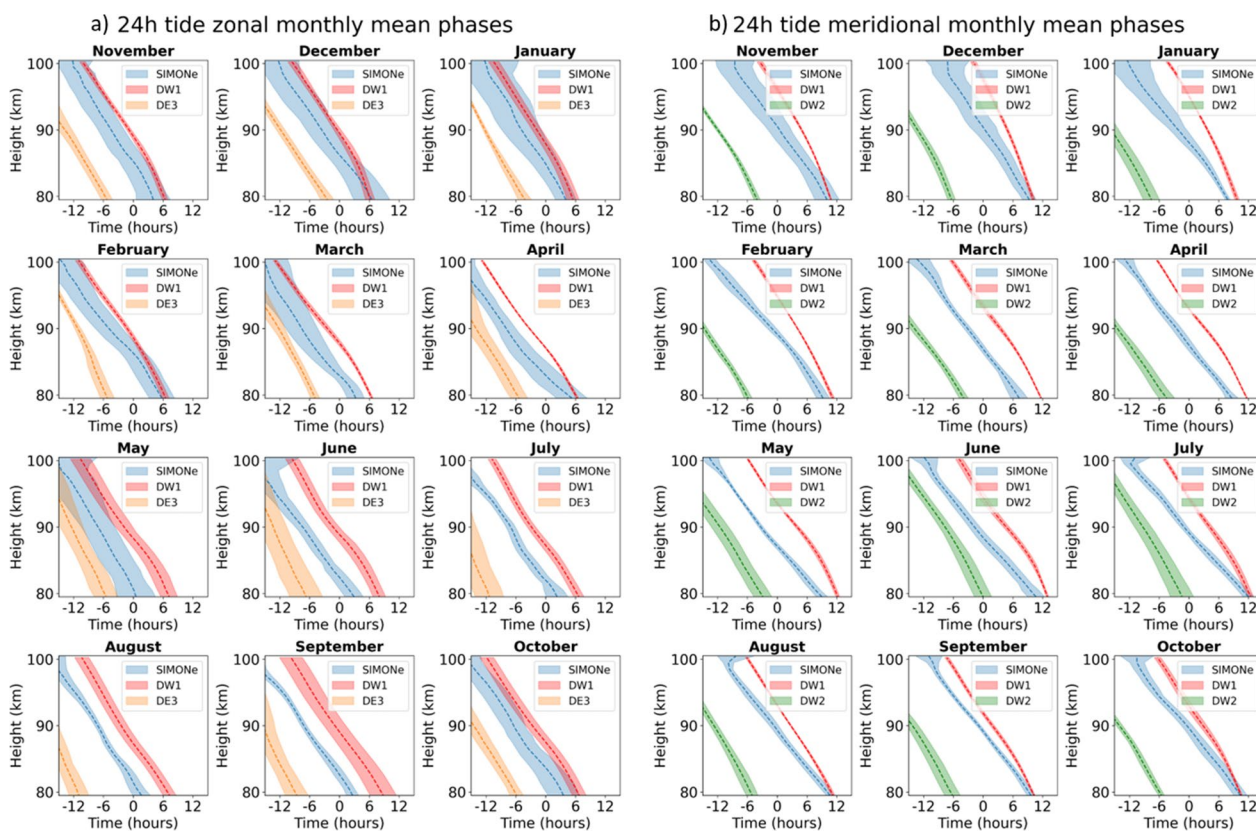


Fig. 3 Monthly phase profiles of the a) zonal and b) meridional component of the 24-h tide for SIMONe observations (blue) and WACCM-X model (DW1 in red, DE3 in orange and DW2 in green). The shaded area shows the maximum day-to-day variability

sion of the mean square norm of the observed climatology by the mean square norm of the composite year of the model. In general, observations and model show low positive correlations; the mean zonal wind and the zonal and meridional components of the 24-h and 8-h tides have the highest correlations (0.4–0.5); these correlations are shown in bold. On average, the correlations (the ratio of amplitudes) between the observations and the model are 0.3 (1.7) for the zonal component and 0.3 (2.0) for the meridional component.

24-h tide amplitudes

Because the dominant wave over Jicamarca is the 24-h tide, the next sections will focus on this tidal component. Figure 2 shows the composite year of the total tide extracted from SIMONe data in the first row and from the WACCM-X model in the second row (same as shown in Fig. 1). From the third to the sixth row, the DW2 (non-migrating), DW1 (migrating), DE1 (non-migrating), and DE3 (non-migrating) tidal components extracted from WACCM-X are respectively shown. The amplitudes of

these four tidal components were obtained using a two-dimensional FFT (in time and longitude) with a window size of 21 days at each given altitude. Other non-migrating diurnal components show negligible amplitudes and hence are not shown.

According to the composite shown in Fig. 2 (notice the different color bars), the main contributions to the zonal component come from DW1 and DE3. In the case of the meridional component, DW1 and DW2 contribute the most. DW1 shows maxima in the equinoxes and minima in the solstices, similarly to the WACCM-X total tide shown in Fig. 1.

Phase profiles of the 24-h tide

The phase profiles of the observed total diurnal tide have been compared with those corresponding to the migrating and dominant non-migrating 24-h tides obtained from the model at the Jicamarca location (taking into account the contribution $2\pi k \lambda_{Jicamarca}/360$ to the phase). Figure 3a, b show the monthly phase profiles for the zonal and meridional components, respectively. The phases for SIMONe data were estimated using the least squares method but applied in bins of 4 days and 1 km, shifted

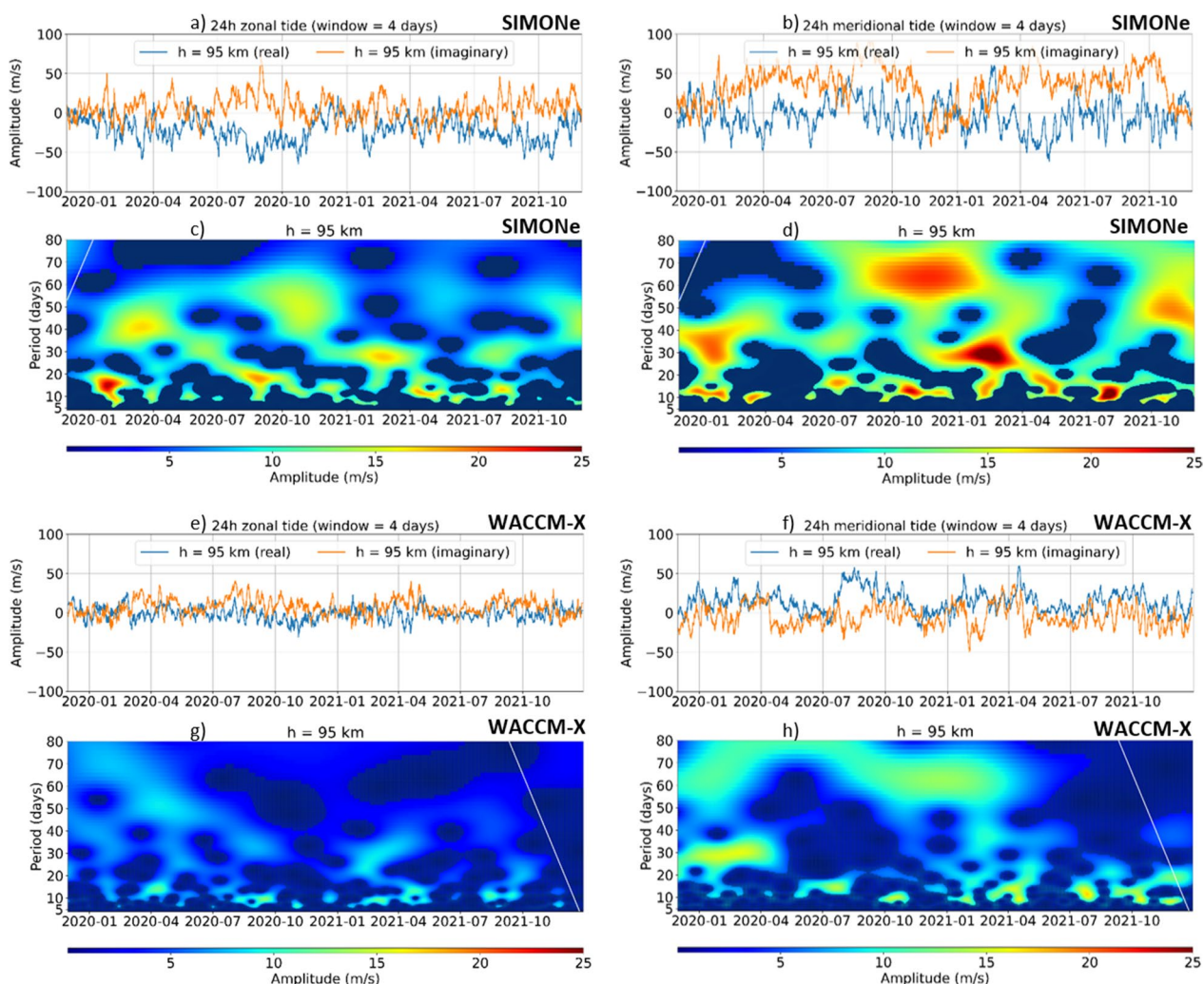


Fig. 4 Modulation of the 24-h tide for the zonal (left) and meridional (right) components at 95 km, from December 2019 until November 2021. The complex amplitudes are shown in **a** and **b**, and the modules of the corresponding CWT are shown in **c** and **d** for SIMONE. **e–f** and **g–h** same as **a–b** and **c–d**, but for WACCM-X. The non-significant levels were blue-darkened to highlight only the 99% significant ones. The white lines mark the cone of influence

by 1 day and 1 km, respectively. The phases for WACCM-X data were estimated using the two-dimensional FFT with a window of 4 days, shifted by 1 day. These estimates were used to compute a yearly climatology with 365 phase values at each altitude. The dashed curve shown in the middle of each colored stripe indicates the median of the phase for that month, and half the stripe’s width corresponds to one standard deviation. This time, a window of 4 days is used to get the day-to-day variability.

Observed and modelled phase profiles show a 24-h tide with decreasing phase in height, which indicates upward propagation. In general, similar values of the vertical wavelength were obtained for the observations from the slope of the phase profiles. These are between 20 and

31 km for the zonal and meridional components. Similar values have been reported in previous studies (e.g., Deepa et al. 2006; Davis et al. 2013). To estimate the vertical wavelength, a straight line is fitted to the monthly phase profile using the least squares method. Then, multiplying the period of the tide (24 h) by the slope value obtained from the fitting yields the vertical wavelength.

In general, the zonal 24-h phase profiles for the observations look like an intermediate profile between those of DW1 and DE3, being closer to and having a very similar slope to DW1 (see Fig. 3a). The zonal observational profiles show less variability from June to September when the phase of DE3 shows a different (higher) slope than that of SIMONE. On the other hand, higher variability

in the SIMONe phase is seen from October until May. Besides, DW1 and DE3 show similar slopes to the observations during those months.

In general, the meridional 24-h phase profiles for the observations show the highest variability from November until January (see Fig. 3b). On the other hand, the lowest variability is seen from February to October. SIMONe profiles look like an intermediate profile between those of DW1 and DW2, being closer to DW1. The observations show equal or slightly smaller slopes than those of DW1 and DW2, which in turn have very similar slopes.

Modulation of the 24-h total tide

To investigate the periods that are coupling (or modulating) the diurnal tide; first, the least squares method was applied with bins of 4 days shifted by 1 day. Then, the complex amplitude of the total diurnal tide was calculated using Eq. 3. Finally, the normalized CWT was applied to these complex amplitudes. Figure 4 shows the results at 95 km for the zonal (meridional) component on the left (right) side, from December 2019 to November 2021. Figure 4a and b show the time series at 95 km (the real part in blue and the imaginary part in orange) and the corresponding modules of the CWT are shown in c and d for SIMONe. Similarly, for WACCM-X data, Figs. 4e and f show the complex amplitudes at 95 km, and the corresponding modules of the CWT are shown in Fig. 4g and h. Only periods between 5 and 80 days are shown.

For the normalized CWT implementation, the wavelet Morlet was used considering the scales as powers of 2, with $L = 15$ levels and $J = 25$ sub-levels per scale (see Eq. 8 in Annex 2). The significance test was applied with a confidence level of 99%, and the non-significant levels were blue-darkened to highlight only the significant ones. The white lines mark the cone of influence.

For the modulation of the observed 24-h zonal component (Fig. 4c), dominant signatures are seen for periods between 6 and 22 days, with peaks around 7–8, 9–12, 13–18, and 18–20 days; and dominant signatures between 25 and 70 days with peaks around 28, 30, 42 and 50 days are also observed. For the modulation of the observed 24-h meridional component (Fig. 4d), dominant signatures for periods between 5 and 20 days, with peaks around 6–8, 9–11, 12–14, and 15–18 days are observed. Other dominant signatures can be seen for periods between 23 and 80 days, with peaks around 30, 35, 50, and 65 days.

For the modulation of the WACCM-X 24-h zonal component (Fig. 4g), dominant signatures for periods between 5 and 22 days, with peaks around 5–7, 8–9, 10–12, 13–15, 18–22 are observed. For periods between

23 and 80 days, clear peaks are seen around 25, 33, 50 and 70 days. In the case of the 24-h meridional component (Fig. 4h), dominant signatures for periods between 6 and 23 days, with peaks around 8, 9–11, 13–15 days, and 18–20 days are observed. For periods between 25 and 80 days, the peaks are clear around 30, 65 and 80 days.

The model shows the presence of similar dominant modulating signatures (periods) but less intense than those of the observations. The ratio of the modulating amplitude peaks between the model and the observations is around 0.6. The modulations in the meridional component have higher amplitudes than in the zonal one.

Discussion

The inter-annual amplitude variability (indicated as contour lines) shown in the observational climatology of the zonal mean wind (U) (Fig. 1a) below 85 km (from September 15 to October 15, from November 15 to 30, and from December 20 to 31) indicates that the changes in the wind direction may occur earlier or later than expected with respect to the climatology. For example, the variability seen between September 15 and October 15 is because in 2020 the winds were eastward, but in the other years they were westward (not shown here). A similar climatology of the mean zonal wind has been found at 8°S by Davis et al. (2013). However, the mean meridional winds (V) we observe below 92 km present more months of southward winds, compared to Davis et al. (2013). The meridional mean winds over Jicamarca are consistent with the pole-to-pole meridional circulation (Strahan 2014). It can be seen that the meridional wind is mostly positive (i.e., equatorward) during the summer months (November to February). During the winter (June to August), it is mostly negative (i.e., poleward).

Similarly to our results (Fig. 1a), the main summer peak of the Q2DW has been observed at other low-latitude locations, for instance, at 7°S and 22°S (Araujo et al. 2014). Moreover, the second peak (March–April) has also been reported at 8°N, 7°S and 22°S as part of sporadic burst events of the Q2DW around the March equinox (Gurubaran et al. (2001); Araujo et al. (2014); Lima et al. (2004) and references therein). Our climatology shows high inter-annual amplitude variability in the second peak (March–April). This is the result of large amplitudes observed in 2022, but rather weak bursts in 2020 and 2021 (not shown here). Differences in climatologies of Q2DW between observations and model simulations (Fig. 1) could be due to the different times used in each case to estimate the composite year. On the other hand, the model has depicted comparable signatures in the summer (January) and winter months (June–July). However, our observations show signatures with low

amplitudes during the winter months (June–August) compared to summer (January). An amplitude behavior similar to our results was observed in Cariri at 7°S (Araujo et al. 2014). On the other hand, we have checked fitting different periods (between 48 and 54 h) to check that our climatology of the Q2DW with the selected period (48 h) is representative.

Davis et al. (2013) reported a semiannual variation in the 24-h tide at 8°S, with a symmetry in the meridional component characterized by maxima at the equinoxes and minima at the solstices. In our observations (Fig. 1a), we do not see that symmetry. In fact, the maximum amplitude in the meridional component is shifted with respect to the September equinox, developing approximately 1 month earlier. On the other hand, the second maximum of the 24-h tide occurs approximately 1 month later, in April–May. In the climatology reported by Wang et al. (2021) at 12°S, 130°E (same latitude as SIMONE Jicamarca), they found that the meridional component of the 24-h tide has a peak in September and another one in February. These differences in the timing of the 24-h tide maxima may indicate that the non-migrating diurnal tidal components contribute (interfere) differently at these two locations (central Peru and northern Australia). Another possibility is that gravity waves enhance in different ways the 24-h tide at these two places (e.g., Yiğit and Medvedev 2017).

In the same study by Davis et al. (2013), they showed a seasonal symmetry in the zonal diurnal tide, with maxima at the equinoxes and minima at the solstices. In our observations, we get an asymmetrical seasonal behavior, with the maximum intensity being reached in August–September (austral spring equinox), and there is no clear maximum in the months around the austral autumn equinox. Also, Wang et al. (2021) show that at 12°S, 130°E the zonal component of the 24-h tide has an asymmetrical seasonal behavior, showing only one peak in February. These differences in the climatology of the total 24-h tide at the same latitudes show the necessity of having more measurements at low latitudes to understand the different contributions from migrating and non-migrating tides.

To double-check that the shift in the diurnal tide peak with respect to equinoxes is not due to the choice of a 21-day window, we employed a 4-day window for computing the diurnal tide amplitudes and after a 21-day running average (not shown here), we verify that there are no changes in the annual cycle, whether a 4-day or 21-day window is used, for both zonal (U) and meridional components (V).

Note that in the first peak of the meridional 24 h-tide (Fig. 1a) between April and the first days of May, there is no variability, but in the case of the second peak between

August and the first days of September, there is high inter-annual variability (15–20 m/s). To get a better climatology and a better characterization of this second peak, more years of data are needed.

The polarization feature of the diurnal tide (i.e., meridional amplitudes larger than the zonal ones) at low latitudes can be explained by taking into consideration the Hough modes (e.g., Forbes 1995). Because the migrating diurnal tide is dominant, we have obtained its Hough functions of the horizontal wind components, zonal U and meridional V (not shown here). They were obtained following the methodology implemented by Wang et al. (2016). We obtained that around 12°S, the ratio V/U is 1.92, which explains the polarization feature in the diurnal tide over Jicamarca during those periods when the migrating diurnal tide is dominant. The periods when the non-migrating tides become more relevant require further analysis, that we leave for future studies.

The observed zonal and meridional 8-h tide maxima (Fig. 1a) occur in months close to autumn and spring equinoxes. The meridional (zonal) component also has a significant signature in June–July (December–January) close to the winter (summer) solstice. For these last signatures, it could be generated by non-linear interaction between diurnal and semidiurnal tides (see Fig. 1a, in December–January (June–July) the zonal (meridional) semidiurnal tide shows significant signatures).

The weak correlations between observations and the model (see Table 1) could be explained due to the lack of a proper gravity wave parameterization in WACCM-X. Unrealistic gravity wave parameterization schemes are a source of uncertainty in the representation of large-scale dynamics of the mesosphere (Smith et al. 2017).

As it is known, the sum of two cosine functions with the same frequency but with different phases is a cosine function with the same frequency, but its new phase is $\tan^{-1} \left[\frac{A \sin(\alpha) + B \sin(\beta)}{A \cos(\alpha) + B \cos(\beta)} \right]$, with A , B and α , β the amplitudes and phases of the original cosines functions. This new phase is a non-linear function. However, since in our case the amplitude of the migrating tide dominates over the non-migrating ones, it is expected that the new phases (the observed total phases) are an intermediate profile between migrating and non-migrating ones, and closer to the one corresponding to the migrating tide. For example, in the zonal phase profile, there is a greater separation between DW1 and SIMONE profiles from June to September (Fig. 3a), which allows us to infer that DE3 is more significant from June to September. Our inference agrees well with the DE3 climatology obtained by satellite observations at Jicamarca latitude (Wu et al. 2008; Wan et al. 2010). Months characterized by large variability in the phase profile, such as January, may suggest high day-to-day variability.

A similar analysis can be made for the meridional component (Fig. 3b); there is a greater separation between DW2 and SIMONE profiles from November to July. Then, we can infer that DW2 is more significant from November to July. However, satellite observations show that DW2 is present most of the months and that there is a minimum from July to September, although with high year-to-year variability (Wu et al. 2008).

Regarding the 24-h total tide modulations (Fig. 4), signatures from less than 25 days could be related to planetary waves which have been observed at low latitudes (e.g., Araujo et al. 2014). The larger periods (greater than 25 days) could correspond to the intra-seasonal oscillations (ISOs) of ~ 60 , ~ 40 and ~ 25 days, similarly to those originally observed by Eckermann and Vincent (1994) and Eckermann et al. (1997) in the MLT region at 2°N . Eckermann et al. (1997) suggested that the Madden–Julian Oscillation (MJO) modulates the intensity of upward-propagating tides. The MJO is a tropical planetary-scale phenomenon eastward-propagated from the Indian Ocean to the Pacific Ocean, and characterized by intraseasonal variability (30–90 days) in tropical winds, pressure, temperature, and rainfall (Zhang et al. 2020).

In general, the zonal and meridional components have different modulating signatures in the observations and the model (see Fig. 4). However, it should be noted that the most intense signatures observed in the meridional component, which occurred around August 2021 with periods of 10–15 days, and January–March 2021 with periods of 25–35 days, show similar signatures in the zonal component (see Fig. 4c and d). The presence of these intense signatures in both components could support the idea of non-linear wave–wave modulation, and they could be interesting cases to study.

Non-linear wave–wave interaction between diurnal tide and planetary waves can be interpreted taking into account the existence of secondary waves with frequencies that are the sum and subtraction of the parent frequencies (e.g., Huang et al. 2013), and also using bi-spectral analysis (e.g., Huang et al. 2013; Mthembu et al. 2013; Kumar et al. 2008; Guharay et al. 2015). Also, some authors have applied spectral analysis to the tide amplitude to show the modulating oscillations (e.g., Dempsey et al. 2021; Guharay et al. 2015; Kumar et al. 2008), but as we point out in Annex 1, the positive envelope does not allow recovering the original modulating signature. To face this problem, we worked with the complex amplitude, which is equivalent to the complex envelope in the context of the Hilbert Transform. Thus, we were able to recover the modulating periods

using the normalized CWT applied to the complex amplitude defined in Eq. (3). Note that this is different than applying CWT to the amplitude, which is equivalent to applying it the magnitude of the complex amplitude, and thus the frequencies are doubled.

Concluding remarks

In this work, the climatology of the horizontal mean winds, solar tides (8, 12, and 24 h), and the Q2DW in the MLT region (80–100 km) over the central coast of Peru (12°S , 77°W) as observed by SIMONE Jicamarca has been presented. Similarly to what it has been reported in some previous studies, the 24-h tide dominates, and its meridional component is more intense than the zonal one. The Q2DW reaches maximum amplitudes during the local summer months, mainly in January.

On the other hand, new features in some parameters are reported. For instance, the second peak observed in the Q2DW between March and April. The 24-h meridional tide presents its maxima shifted with respect to the equinox times (the largest peak occurs in August–September, and the second one occurs in April–May), and the zonal component only shows a clear maximum in August–September.

Furthermore, the shifting of the peaks with respect to equinoxes is most likely due to different contributions from non-migrating diurnal tides, as well as locally enhanced gravity wave activity. Thus, our observations can be of help for the modelling community to improve the representation of different tidal wave numbers, as well as for tuning their gravity wave parameterization schemes to see if changes in the gravity wave activity result in changes in the temporal evolution of the diurnal tide at MLT altitudes.

Comparison of the climatology between observations and the WACCM-X model shows a weak correlation (0.3). The highest correlations (0.4–0.5) are reached for the zonal and meridional components of the 24-h and 8-h tides, and the zonal mean wind. On average, model amplitudes are 50% smaller than the observed ones.

Concerning the 24-h tide, our analysis of the observed tidal phases in comparison with those extracted from WACCM-X (Fig. 3) has allowed us to infer that the migrating component (DW1) is dominant, but it is shown that from June to September (from November to July), the DE3 (DW2) may have a significant contribution to the observed zonal (meridional) 24-h total tide. The results that came out of this approach are in agreement with previous studies based on satellite observations, which tells us that the approach is valid. Furthermore, our approach could be used in shorter time scales (a few days, instead of a month), which would not be possible

using satellite observations since they are usually averaged over 45 days or more, to extract information on tides.

Finally, it has been defined a complex amplitude to study the modulations of the 24-h total tide. Modulating signatures with periods between 5 and 80 days, most likely due to planetary waves and intraseasonal oscillations (large-scale tropospheric oscillation), have been reported in both the SIMONE observations and the WACCM-X model. The modulations in the meridional component have larger amplitudes than in the zonal one.

Annex 1

Considering a non-linear wave-wave interaction given by:

$$x(t) = m(t)\text{Cos}(2\pi f_c t + \phi_c), \tag{4}$$

where f_c and ϕ_c are the frequency and phase of the carrier (the diurnal tide in our study), $m(t)$ is a real function that corresponds to the modulated amplitude by the oscillations with large periods (e.g., $m(t) = A_p \text{Cos}(2\pi f_p t + \phi_p)$, where f_p and ϕ_p are the frequency and phase of planetary waves).

Let $x(t)$ be a real function, its Hilbert transform (Chapter 4., Feldman 2011) is $x_h(t) = x(t) \otimes \frac{1}{\pi t}$. Then, the analytic signal is defined as: $x_a(t) = x(t) + jx_h(t)$, and the complex envelope is defined as: $\tilde{x}(t) = x_a(t)e^{-j2\pi f_c t}$. It is known that for the $x(t)$ considered in Eq. 4, the module of the analytic signal allows recovering the envelope (always positive) of $x(t)$. It is the module of the modulated signal ($|x_a(t)| = |m(t)|$), but if we want to recover the source of the modulating signal, it is better to work with the complex envelope whose spectrum has the same frequency and amplitude information of $m(t)$'s spectrum but with a shifted phase.

Thus, for the $x(t)$ signal given in (4), we have $x_a(t) = m(t)e^{j(2\pi f_c t + \phi_c)}$, and

$$\tilde{x}(t) = m(t)e^{j\phi_c} = m(t)\text{Cos}(\phi_c) + jm(t)\text{Sin}(\phi_c). \tag{5}$$

As we can see, when we are taking the complex time series $A_q - jB_q$ obtained by least squares (Eq. 1), we are actually generating the complex envelope (taking into account the negative sign in the phase).

Annex 2

The CWT is optimal for locating non-stationary signals, specifically high frequencies with rapid variations and low frequencies with slow variations (Gao and Yan 2010). Given a signal $f(t)$, the CWT is defined as

$$WT(s, t) = \langle f, \psi_{s,t} \rangle = \int_{-\infty}^{+\infty} f(t') \frac{2}{\sqrt{2\pi s}} \psi^* \left(\frac{t' - t}{s} \right) dt'; \tag{6}$$

where t is the time, and s is the selected scale.

This definition allows the module of the CWT to recover the original amplitude of sinusoidal harmonic components of the analyzed signal. This definition is equivalent to that given by Liu et al. (2007) for a normalized CWT.

In this work, we consider the wavelet Morlet $\psi(t) = e^{i\omega_0 t} e^{-\frac{t^2}{2}}$, whose Fourier Transform, $\hat{\psi}(\omega) = \sqrt{2\pi} e^{-\frac{1}{2}(\omega - \omega_0)^2}$, is considered with $\omega_0 = 6$ (Torrence and Compo 1998). From the convolution theorem, it follows:

$$WT(s, t) = f(t) \otimes \frac{2}{\sqrt{2\pi s}} \psi^* \left(\frac{-t}{s} \right) = \mathcal{F}^{-1} \left(\hat{f}(\omega) \frac{2}{\sqrt{2\pi}} [\hat{\psi}(s\omega)]^* \right), \tag{7}$$

where \otimes is the convolution operator; * indicates the complex conjugate; and \mathcal{F}^{-1} is the inverse Fourier transform.

For $f(t)$ sampled at $t = n\Delta t$ points ($n = 0, 1, 2, \dots$), i.e., the discrete signal $f[n]$, one has

$$WT_{f\psi}(s, n) = \mathcal{F}^{-1} \left(\hat{f} \left[\frac{2\pi k}{N\Delta t} \right] \frac{2}{\sqrt{2\pi}} \left[\hat{\psi} \left[s \frac{2\pi k}{N\Delta t} \right] \right]^* \right). \tag{8}$$

The discretized time and frequency are $t = n\Delta t$ and $\omega_k = \frac{2\pi k}{N\Delta t}$, with n and $k = 0, 1, 2, \dots, N - 1$. For the wavelet Morlet, the relation between the scale "s" and the equivalent Fourier period is

$$T_{CWT} = \frac{4\pi s}{\omega_0 + \sqrt{\omega_0^2 + 2}} \text{ (Torrence and Compo 1998)}.$$

Scales s_j are selected as powers of 2 with sub-levels J and the number of levels equal to L:

$$s_j = (2\Delta t) * 2^j, \quad \text{with } j = 0, 1, 2, \dots, j_{max}, \quad \text{where } j_{max} = LJ.$$

To implement the significance test of the wavelet power, we have used a Gaussian White Noise process as the background distribution presumed (see section 3.1 in Ge et al. (2007)). The cone of influence was obtained similarly as Torrence and Compo (1998).

Abbreviations

MLT	Mesosphere and Lower Thermosphere
IAP	Leibniz-Institute of Atmospheric Physics
SIMONE	Spread spectrum Interferometric Multistatic meteor radar Observing Network
Q2DW	Quasi-two-Day Wave
WACCM-X	Specified dynamics Whole Atmosphere Community Climate Model with thermosphere-onesphere
X	eXtension

Acknowledgements

The authors thank the staff at the Radio Observatory of Jicamarca for their support and help in maintaining SIMOne Jicamarca. J.S. thanks Dr. Miguel Urco for the discussions about signal processing.

Author contributions

Conceptualization, JS, JLC, MM and JFC; methodology, JS and JLC; formal analysis, JS, JLC, MM and JFC; software, JS; writing—original draft preparation, JS; writing—review and editing, JS, JFC, JLC, MM, NP, and KK; All authors have read and agreed to the published version of the manuscript.

Funding

We acknowledge ProCiencia for the support/financing under agreement No 075-2021-FONDECYT. In addition, we acknowledge high-performance computing support from Cheyenne (<https://doi.org/10.5065/D6RX99HX>) provided by NCAR's Computational and Information Systems Laboratory. This material is based upon work supported by the National Center for Atmospheric Research, which is a major facility sponsored by the U.S. National Science Foundation under Cooperative Agreement 1852977.

Availability of data and materials

The data used to produce the SIMOne radar results is available in HDF5 format at <https://www.radar-service.eu/radar/en/dataset/citoY00FRhuOeJtS?token=XAcPMMSiKELqoiLkTNg0>. All the winds from WACCM-X model used in this work can be found in <https://doi.org/10.26024/5b58-nc53>

Declarations

Competing interests

The authors declare that they have no competing interests.

Author details

¹Leibniz Institute of Atmospheric Physics at the University of Rostock, Kühlungsborn, Germany. ²Sección de Electricidad y Electrónica, Pontificia Universidad Católica del Perú, Lima, Peru. ³High Altitude Observatory, National Center for Atmospheric Research, Boulder, CO, USA. ⁴Radio Observatorio de Jicamarca, Instituto Geofísico del Perú, Lima, Peru.

Received: 30 May 2023 Accepted: 9 November 2023

Published online: 14 December 2023

References

- Araújo LR, Lima LM, Batista PP, Clemesha BR, Takahashi H (2014, May) Planetary wave seasonality from meteor wind measurements at 7.4 S and 22.7 S. In *Annales Geophysicae* (Vol. 32, No. 5, pp. 519–531). Göttingen, Germany: Copernicus Publications. <https://doi.org/10.5194/angeo-32-519-2014>
- Chau JL, Hoffmann P, Pedatella NM, Matthias V, Stober G (2015) Upper mesospheric lunar tides over middle and high latitudes during sudden stratospheric warming events. *J Geophys Res Space Phys* 120(4):3084–3096. <https://doi.org/10.1002/2015JA020998>
- Chau JL, Urco JM, Vierinen J, Harding BJ, Clahsen M, Pfeffer N, Erickson PJ (2021) Multistatic specular meteor radar network in Peru: System description and initial results. *Earth and Space Science* 8(1):e2020JD033822. <https://doi.org/10.1029/2020EA001293>
- Conte JF, Chau JL, Stober G, Pedatella N, Maute A, Hoffmann P, Murphy DJ (2017) Climatology of semidiurnal lunar and solar tides at middle and high latitudes: interhemispheric comparison. *J Geophys Res Space Phys* 122(7):7750–7760. <https://doi.org/10.1002/2017JA024396>
- Conte JF, Chau JL, Urco JM, Latteck R, Vierinen J, Salvador JO (2021) First studies of mesosphere and lower thermosphere dynamics using a multistatic specular meteor radar network over southern Patagonia. *Earth Space Sci*. <https://doi.org/10.1029/2020EA001356>
- Davis RN, Du J, Smith AK, Ward WE, Mitchell NJ (2013) The diurnal and semidiurnal tides over Ascension Island (8° S, 14° W) and their interaction with the stratospheric quasi-biennial oscillation: studies with meteor radar, eCMAM and WACCM. *Atmos Chem Phys* 13(18):9543–9564. <https://doi.org/10.5194/acp-13-9543-2013>
- Deepa V, Ramkumar G, Antonita M, Kumar KK, Sasi MN (2006, November) Vertical propagation characteristics and seasonal variability of tidal wind oscillations in the MLT region over Trivandrum (8.5 N, 77 E): First results from SKiYMET meteor radar. In *Annales Geophysicae* (Vol. 24, No. 11, pp. 2877–2889). Göttingen, Germany: Copernicus Publications
- Dempsey SM, Hindley NP, Moffat-Griffin T, Wright CJ, Smith AK, Du J, Mitchell NJ (2021) Winds and tides of the Antarctic mesosphere and lower thermosphere: one year of meteor-radar observations over Rothera (68 S, 68 W) and comparisons with WACCM and eCMAM. *J Atmos Solar Terr Phys* 212:105510. <https://doi.org/10.1016/j.jastp.2020.105510>
- Eckermann SD, Vincent RA (1994) First observations of intraseasonal oscillations in the equatorial mesosphere and lower thermosphere. *Geophys Res Lett* 21(4):265–268
- Eckermann SD, Rajopadhyaya DK, Vincent RA (1997) Intraseasonal wind variability in the equatorial mesosphere and lower thermosphere: long-term observations from the central Pacific. *J Atmos Solar Terr Phys* 59(6):603–627. [https://doi.org/10.1016/S1364-6826\(96\)00143-5](https://doi.org/10.1016/S1364-6826(96)00143-5)
- Feldman M (2011) Hilbert transform applications in mechanical vibration. John Wiley & Sons
- Forbes JM (1995) Tidal and planetary waves. *Upper Mesosphere Lower Thermosphere Rev Exp Theory* 87:67–87. <https://doi.org/10.1029/GM087p0067>
- Gao RX, Yan R (2010) Wavelets: Theory and applications for manufacturing. Springer Science & Business Media
- Ge Z (2007, November) Significance tests for the wavelet power and the wavelet power spectrum. In *Annales Geophysicae* (Vol. 25, No. 11, pp. 2259–2269). Göttingen, Germany: Copernicus Publications
- Guharay A, Batista PP, Clemesha BR (2015) On the variability of the diurnal tide and coupling with planetary waves in the MLT over Cachoeira Paulista (22.7 S, 45 W). *J Atmos Solar Terr Phys* 133:7–17. <https://doi.org/10.1016/j.jastp.2015.07.016>
- Gurubaran S, Sridharan S, Ramkumar TK, Rajaram R (2001) The mesospheric quasi-2-day wave over Tirunelveli (8.7 N). *J Atmos Solar Terr Phys* 63(10):975–985. [https://doi.org/10.1016/S1364-6826\(01\)00016-5](https://doi.org/10.1016/S1364-6826(01)00016-5)
- Hagan ME (1996) Comparative effects of migrating solar sources on tidal signatures in the middle and upper atmosphere. *J Geophys Res Atmos* 101(D16):21213–21222. <https://doi.org/10.1029/96JD01374>
- Hagan ME, Forbes JM (2003) Migrating and nonmigrating semidiurnal tides in the upper atmosphere excited by tropospheric latent heat release. *J Geophys Res Space Phys*. <https://doi.org/10.1029/2002JA009466>
- He M, Chau JL, Forbes JM, Zhang X, Englert CR, Harding BJ, Makela JJ (2021) Quasi-2-day wave in low-latitude atmospheric winds as viewed from the ground and space during January–March, 2020. *Geophys Res Lett*. <https://doi.org/10.1029/2021GL093466>
- Huang KM, Liu AZ, Zhang SD, Yi F, Huang CM, Gan Q, Zhang YH (2013, November) A nonlinear interaction event between a 16-day wave and a diurnal tide from meteor radar observations. In *Annales Geophysicae* (Vol. 31, No. 11, pp. 2039–2048). Göttingen, Germany: Copernicus Publications. <https://doi.org/10.5194/angeo-31-2039-2013>
- Kumar KK, Deepa V, Antonita TM, Ramkumar G (2008) Meteor radar observations of short-term tidal variabilities in the low-latitude mesosphere-lower thermosphere: Evidence for nonlinear wave-wave interactions. *Journal of Geophysical Research: Atmospheres*, 113(D16)
- Kumar GK, Singer W, Oberheide J, Grieger N, Batista PP, Rigglin DM, Clemesha BR (2014) Diurnal tides at low latitudes: radar, satellite, and model results. *J Atmos Solar Terr Phys* 118:96–105. <https://doi.org/10.1016/j.jastp.2013.07.005>
- Laštovička J (2006) Forcing of the ionosphere by waves from below. *J Atmos Solar Terr Phys* 68(3–5):479–497. <https://doi.org/10.1016/j.jastp.2005.01.018>
- Lima LM, Batista PP, Takahashi H, Clemesha BR (2004) Quasi-two-day wave observed by meteor radar at 22.7 S. *J Atmos Solar Terr Phys* 66(6–9):529–537. <https://doi.org/10.1016/j.jastp.2004.01.007>
- Liu L, Hsu H, Grafarend EW (2007) Normal Morlet wavelet transform and its application to the earth's polar motion. *J Geophys Res Solid Earth*. <https://doi.org/10.1029/2006JB004895>
- Mthembu SH, Sivakumar V, Mitchell NJ, Malinga SB (2013) Studies on planetary waves and tide interaction in the mesosphere/lower thermosphere region using meteor RADAR data from Rothera (68 S, 68 W), Antarctica. *J Atmos Solar Terr Phys* 102:59–70

- Pedatella NM, Liu HL, Conte JF, Chau JL, Hall C, Jacobi C, Tsutsumi M (2021) Migrating semidiurnal tide during the September equinox transition in the Northern Hemisphere. *J Geophys Res Atmos* 126(3):e2020JD033822. <https://doi.org/10.1029/2020JD033822>
- Sandford DJ, Mitchell NJ (2007, February) Lunar tides in the Mesosphere over Ascension Island (8° S, 14.4° W). In *Annales Geophysicae* (Vol. 25, No. 1, pp. 9–12). Göttingen, Germany: Copernicus Publications. <https://doi.org/10.5194/angeo-25-9-2007>
- Smith AK (2012) Global dynamics of the MLT. *Surv Geophys* 33:1177–1230
- Smith AK, Pedatella NM, Marsh DR, Matsuo T (2017) On the dynamical control of the mesosphere-lower thermosphere by the lower and middle atmosphere. *J Atmos Sci* 74(3):933–947. <https://doi.org/10.1175/JAS-D-16-0226.1>
- Strahan SE (2014) MIDDLE ATMOSPHERE | Transport Circulation, Editor(s): Gerald R. North, John Pyle, Fuqing Zhang, *Encyclopedia of Atmospheric Sciences* (Second Edition), Academic Press, 2015, Pages 41–49, ISBN 9780123822253, <https://doi.org/10.1016/B978-0-12-382225-3.00231-0>
- Thomson RE, Emery WJ (2014) *Data analysis methods in physical oceanography*. Newnes
- Torrence C, Compo GP (1998) A practical guide to wavelet analysis. *Bull Am Meteorol Soc* 79(1):61–78
- Wang H, Boyd JP, Akmaev RA (2016) On computation of Hough functions. *Geosci Model Dev* 9(4):1477–1488. <https://doi.org/10.5194/gmd-9-1477-2016>
- Wang J, Yi W, Wu J, Chen T, Xue X, Vincent RA, Dou X (2021) Climatology of migrating and non-migrating tides observed by three meteor radars in the southern equatorial region. *Atmos Chem Phys Discuss*. <https://doi.org/10.5194/acp-2021-33>
- Wan W, Xiong J, Ren Z, Liu L, Zhang ML, Ding F, Ning B, Zhao B, Yue X (2010) Correlation between the ionospheric WN4 signature and the upper atmospheric DE3 tide. *Journal of Geophysical Research: Space Physics*, 115(A11)
- Wu Q, Ortland DA, Killeen TL, Roble RG, Hagan ME, Liu H-L, Solomon SC, Jiyao Xu, Skinner WR, Nijicjewski RJ (2008) Global distribution and interannual variations of mesospheric and lower thermospheric neutral wind diurnal tide: 2. Nonmigrating tide. *J Geophys Res Space Phys*. <https://doi.org/10.1029/2007JA012543>
- Yiğit E, Medvedev AS (2017) Influence of parameterized small-scale gravity waves on the migrating diurnal tide in earth's thermosphere. *J Geophys Res Space Phys* 122:4846–4864
- Zhang C, Adames ÁF, Khouider B, Wang B, Yang D (2020) Four theories of the Madden-Julian oscillation. *Rev Geophys*. <https://doi.org/10.1029/2019RG000685>

Publisher's Note

Springer Nature remains neutral with regard to jurisdictional claims in published maps and institutional affiliations.

Submit your manuscript to a SpringerOpen[®] journal and benefit from:

- Convenient online submission
- Rigorous peer review
- Open access: articles freely available online
- High visibility within the field
- Retaining the copyright to your article

Submit your next manuscript at ► [springeropen.com](https://www.springeropen.com)
